Dynamic cerebrovascular autoregulation in patients prone to postural syncope: comparison of techniques assessing the autoregulation index from spontaneous variability series

Francesca Gelpi[1], Vlasta Bari[1], Beatrice Cairo[1,2], Beatrice De Maria[3], Davide Tonon[4], Gianluca Rossato[4], Luca Faes[5], Alberto Porta[1,2]

[1]Department of Cardiothoracic, Vascular Anesthesia and Intensive Care, IRCCS Policlinico San Donato, San Donato Milanese, Milan, Italy

[1]Department of Biomedical Sciences for Health, University of Milan, Milan, Italy

[3]IRCCS Istituti Clinici Scientifici Maugeri, Milan, Italy

[4]Department of Neurology, IRCCS Sacro Cuore Don Calabria Hospital, Negrar, Verona, Italy

[5]Department of Engineering, University of Palermo, Palermo, Italy

Running title: Orthostatic stressor and cerebrovascular autoregulation

Address for correspondence:

Prof. Alberto Porta, PhD
Università degli Studi di Milano
Dipartimento di Scienze Biomediche per la Salute
IRCCS Policlinico San Donato
Laboratorio di Modellistica di Sistemi Complessi
Via F. Fellini 4
20097, San Donato Milanese
Milano, Italy

Tel: +39 02 52774382
Fax: +39 02 50319979
Email: alberto.porta@unimi.it

Abstract

Three approaches to the assessment of cerebrovascular autoregulation (CA) via the computation of the autoregulation index (ARI) from spontaneous variability of mean arterial pressure (MAP) and mean cerebral blood flow velocity (MCBFV) were applied: 1) a time domain method (TDM) assessing the similarity between the original MCBFV and the version generated by the Tiecks' model driven by the original MAP; 2) two procedures based on the agreement of the impulse response of the pressure-to-flow transfer function estimated via nonparametric method (nonPM) and parametric method (PM) respectively with the one of the Tiecks' model. Performances were tested over matched pairs and unmatched couples artificially created by randomly associating a MAP series taken from one subject with a MCBFV series taken from another. Data were analyzed at supine resting (REST) and during the early phase of 60° head-up tilt (TILT) in 13 subjects with previous history of postural syncope (SYNC, age: 28 ±9 yrs; 5 males) and 13 control individuals (nonSYNC, age: 27 ± 8 yrs; 5 males). Analysis was completed by computing autonomic markers from heart period (HP) and systolic arterial pressure (SAP) variability series, namely the high frequency (HF) power of HP series (HF_{HP}) and the low frequency (LF) power of SAP series (LF_{SAP}). HP and SAP spectral indexes suggested that nonSYNC and SYNC groups exhibited different autonomic responses to TILT being HF_{HP} significantly decreased solely in SYNC and LF_{SAP} significantly increased exclusively in nonSYNC group. ARI analysis suggested that: i) both TDM and PM have a sufficient statistical power to separate matched from unmatched pairs; ii) TDM should be preferred to PM because it has a greater flexibility in identifying different types of CA; iii) MCBFV significantly decreased during TILT in both populations but the orthostatic stressor did not induce any evident CA impairment in either nonSYNC or SYNC individuals. We conclude that modification of autonomic state imposed by TILT and the different autonomic response to postural challenge in nonSYNC and SYNC subjects were not able to produce any modification of dynamic component of the CA.

Keywords: heart rate variability, arterial pressure, mean cerebral blood flow velocity, head-up tilt; cardiovascular control; autonomic nervous system.

1. Introduction

Cerebrovascular autoregulation (CA) is the physiological mechanism that maintains an approximately constant cerebral blood flow (CBF) by actively counter-regulating the vessel diameter in response to arterial pressure (AP) changes in the range of 60-150 mmHg (Lassen, 1959). Historically, static CA was assessed after the inhalation of nitrous oxide (Kety and Schmidt, 1948) or Xenon 133 (Obrist et al., 1975) through the application of the Fick principle. With the development of transcranial Doppler ultrasound device (Aaslid et al., 1989), static CA evaluation was carried out more easily by inducing mean AP (MAP) modification through an intervention, such as a pharmacological challenge (Tiecks et al., 1995), and by observing the steady state response of mean cerebral blood flow (MCBF) as evaluated from its proxy, i.e. MCBF velocity (MCBFV), under the hypothesis of constancy of the diameter of the insonated vessel. More importantly, transcranial Doppler ultrasound device (Aaslid et al., 1989) provides a sufficient time resolution to assess of CA dynamic properties by following over time the MCBFV adjustments to a sudden, and relevant, modification of MAP, such as after thigh cuff release, and by characterizing type and shape of the resulting MCBFV transient (Tiecks et al., 1995). The dynamic CA markers complement static CA indexes because they provide indications that cannot be inferred from static CA analysis about the efficiency of CA mechanisms such as rapidity to return to basal value. Dynamic CA analysis was originally associated to interventions necessary to provoke a sudden and important modification of MAP (Tiecks et al., 1995). In the attempt to enlarge the possibility of assessing dynamic CA in subjects that might be at risk when artificial, and relevant, AP changes are induced, methods exploiting spontaneous fluctuations of MAP and MCBFV were devised (Claassen et al., 2016). A class of these methods (Panerai et al., 1998; Panerai et al., 1999) is based on a modeling approach describing the CA as a derivative filter that was originally developed by Tiecks et al., (1995) in the context of interventional procedure of CA assessment (Aaslid et al., 1989). The Tiecks' model provided a set of impulse responses that are graded according to the value of an autoregulatory index (ARI) typifying the efficiency in performing CA from 0, i.e. absent CA, to 9, i.e. excellent CA, being 5 the limit between impaired and intact CA (Tiecks et al., 1995). The similarity between the impulse response derived from the Tiecks' model and that obtained from spontaneous variations of MAP and MCBFV via a nonparametric method (nonPM) based on Fourier transformation (Panerai et al., 1998) or a parametric method (PM) via modeling approach (Panerai et al., 1999; Simpson et al., 2001; Dineen et al., 2010) was evaluated as a function of ARI with the aim at selecting the impulse response that provides the best agreement with real data and at storing the associated ARI. This approach was extremely successful in typifying CA from spontaneous variability recordings of MAP and MCBFV in several protocols and/or groups of

individuals (Panerai et al., 1998; Carey et al., 2001; Panerai et al., 2001; Dineen et al., 2010; Castro et al., 2014; Claassen et al., 2016). However, a simpler, and apparently more intuitive time domain method (TDM), would be to directly feed the differential equations of the Tiecks' model with the spontaneous variations of MAP, let the MAP dynamics evolve over time and identify the model response that best fits the measured MCBFV (Mahdi et al., 2017; Lee et al., 2020). This method might be more robust given that it does not require the computation of the transfer function leading to typical issues of the frequency domain analysis such as the choice of frequency resolution and superior cut-off of the frequency representation and the magnitude of the link between the input and output signals affecting the ability of the model to deal with noise at high frequency and reliability of the description of the MAP-MCBFV relationship.

Several studies exploited orthostatic stressors in the attempt to elucidate the role played by autonomic nervous system (ANS) in governing CA (Grubb et al., 1991; Levine et al., 1994; Bondar et al., 1995; Lefthériotis et al., 1998; Zhang et al., 1998; Carey et al., 2001; Panerai et al., 2001; Schondorf et al., 2001; Carey et al., 2003; Castro et al., 2017). A relevant portion of them are based on the computation of ARI (Carey et al., 2001; Panerai et al., 2001; Carey et al., 2003; Castro et al., 2017). Therefore, details in the assessment of CA via ARI approach might play a fundamental role in shaping conclusions. Moreover, given that vasoconstriction imposed by sympathetic activation reduces vessel diameter and vasoconstriction episodes might contribute to reduce CBF whether they do not occur in synchrony with suitable AP rises (Grubb et al., 1991; Cassaglia et al., 2008), it remains matter of debate whether sympathetic activation observed during orthostatic challenge (Montano et al., 1994; Cooke et al., 1999; Furlan et al., 2000; Marchi et al., 2016) is helpful or detrimental to the CA preservation. Moreover, it is also unclear whether different autonomic control responses to the postural challenges such as those typically observed in SYNC and nonSYNC groups (Piccirillo et al., 2004; Folino et al., 2007; Furlan et al., 2019) could result in different CA patterns.

In the present study we compare three approaches to the quantification of CA from spontaneous variability of MAP and MCBFV, namely a TDM searching the best matching over time between MCBFV predicted from the Tiecks' differential equations driven by the recorded MAP and the MCBFV original series (Mahdi et al., 2017), and two techniques searching for the best matching between the impulse response derived from the Tiecks' model and the one estimated via nonPM (Panerai et al., 1998) and PM (Panerai et al., 1999). The TDM, nonPM and PM were tested over MAP and MCBFV recorded during an orthostatic challenge in subjects with recurring episodes of syncope compared to a control population.

2. Methods

2.1 Assessing ARI via TDM

The TDM was originally proposed in (Mahdi et al., 2017). The beat-to-beat MAP series were first resampled at f=10 Hz. The resulting time-domain series was normalized as

$$dMAP_k = \frac{MAP_k - MAP_{mean}}{MAP_{mean} - \mathrm{P_{cr}}}, \qquad (1)$$

where MAP_{mean} is the mean of MAP over the selected sequence, $\mathrm{P_{cr}}$ is the is the critical closing pressure set to 12 mmHg and k is the current time. The approach exploits the derivative filter originally developed in (Tiecks et al., 1995) describing the dynamical link from dMAP to dMCBFV. The Tiecks' model consists in the discretized differential equations operating over the state variable x_1 and x_2 as

$$x_{1,k} = x_{1,k-1} + \frac{dMAP_k - x_{2,k-1}}{f \cdot T}, \qquad (2)$$

and

$$x_{2,k} = x_{2,k-1} + \frac{x_{1,k-1} - 2 \cdot D \cdot x_{2,k-1}}{f \cdot T}, \qquad (3)$$

where MAP_k is the input of the filter, f is the resampling frequency, D is the damping coefficient, and T is the time constant, while the output is computed as

$$MCBFV_k = MCBFV_{mean} \cdot (1 + dMAP_k + K \cdot x_{2,k}), \qquad (4)$$

where $MCBFV_{mean}$ is the mean of MCBFV over the selected sequence input and K is the gain. The initial conditions were set as $x_{1,0}$=2·D·dMAP$_0$ and $x_{2,0}$=dMAP$_0$. According to the value set for K, T and D ten combinations of the triplet K, T and D was chosen in (Tiecks et al., 1995). Each combination was symbolized by a value of ARI grading situations ranging from absent CA (i.e. ARI = 0) to excellent CA (ARI = 9). The predicated MCBFV, generated using (4) after feeding it with the original dMAP and x_2 obtained via the (2) and (3), was compared with the measured MCBFV using the normalized mean square prediction error (NMSPE), namely the mean square value of the difference between the predicted MCBFV and measured MCBFV normalized by the mean square value of the measured MCBFV (Angarita-Jaimes et al., 2010). We selected the ARI corresponds to the curve that provide the minimum of the NMSPE. The optimal ARI derived from this approach was labelled $\mathrm{ARI_{TDM}}$.

2.2 Assessing ARI from the impulse response derived via nonPM

The nonPM was originally proposed in (Panerai et al., 1998). The beat-to-beat MAP and MCBFV variability series were first resampled at f=10 Hz. The resulting MAP and MCBFV series were normalized as

$$dMAP_k = \frac{MAP_k - MAP_{mean}}{MAP_{mean}} \qquad (5)$$

and

$$dMCBFV_k = \frac{MCBFV_k - MCBFV_{mean}}{MCBFV_{mean}} \qquad (6)$$

where MAP_{mean} and $MCBFV_{mean}$ are the means of MAP and MCBFV respectively and k is the current time. Transfer function was computed as the ratio of dMCBFV-dMAP cross-spectrum to the dMAP power spectrum. Cross-spectrum was estimated as the product of the Fourier transform of the dMAP series times the complex conjugation of the Fourier transform of the dMCBFV series while the power spectrum of dMAP as the square of the Fourier transform modulus of the dMAP. The inverse Fourier transformation was applied to the transfer function to derive the impulse response. The approach exploits the impulse responses derived from Tiecks' model according to the ten combinations of K, T and D proposed by Tiecks et al. (1995). The method compares impulse response predicted by the analysis of dMAP and dMCBFV variability to the theoretical impulse responses searching for the curve providing the minimum of the NMSPE. The theoretical impulse response was derived by differentiating the Tiecks' model response to a unity sustained step. Theoretical and predicted impulse responses were rescaled by dividing each sample by their own maximum absolute value. The ARI corresponding to the NMSPE minimum was labelled ARI_{nonPM}. Since CA effects should be exhausted by a few seconds (Zhang et al., 1998), comparison between predicted and theoretical impulse responses was carried out over 3 s (Panerai et al., 1998).

2.3 Assessing ARI from the impulse response derived via PM

Linear and nonlinear parametric models were applied to describe the MCBFV-MAP relation (Panerai et al., 1999). In the present study we applied an autoregressive (AR) model with exogenous (X) input (ARX) to describe the dynamical evolution of MCBFV driven by MAP changes (Porta et al., 2000; Porta et al., 2018). After the application of a linear detrending to both MCBFV and MAP, the current $MCBFV_k$ was described as the linear combination of p past MCBFVs weighted by the coefficients a_i, with i=1, …, p plus the linear combination of $p-\tau+1$ past MAPs, including possibly the current one if τ=0, weighted by the coefficients b_i, with i=τ, …, p plus a random unpredictable portion W_k, being the sampling of a Gaussian white noise W with zero mean and variance λ^2, namely

$$MCBFV_k = \sum_{i=1}^{p} a_i \cdot MCBFV_{k-i} + \sum_{i=\tau}^{p} b_i \cdot MAP_{k-i} + W_k \,, \qquad (7)$$

where p is the model order and τ is the delay of the actions from MAP to MCBFV. The delay τ from MAP to MCBFV was set to 0 beats to allow the description of the fast actions that might be present

whether the resistance contributions to MBCFV changes are dominant over the capacitance ones (Kontos, 1989; Tzeng et al., 2014). The (7) can be rewritten using the one delay operator z^{-1} in the Z-domain defined as $MCBFV_{k-1}=z^{-1}\cdot MCBFV_k$ and $MAP_{k-1}=z^{-1}\cdot MAP_k$ as

$$MCBFV_k = A(z)\cdot MCBFV_k + B(z)\cdot MAP_k + W_k\,, \qquad (8)$$

where $A(z)=\sum_{i=1}^{p} a_i\cdot z^{-i}$ and $B(z)=\sum_{i=\tau}^{p} b_i\cdot z^{-i}$ are polynomials with constant coefficients in z^{-1}. The transfer function $H_{MCBFV\text{-}MAP}(z)$ from MAP to MCBFV is given by

$$H_{MCBFV\text{-}MAP}=\frac{B(z)}{1-A(z)}\,. \qquad (9)$$

The long division of $B(z)$ to $1-A(z)$ provides the coefficients of the impulse response. The impulse response was trunked to 31 values from cardiac beat 0 to 30. Temporal index was converted into time by multiplying it by the heart period (HP) mean. The impulse response was resampled at f=10 Hz and compared to the impulse responses derived from the Tiecks' model as described in *Sect.2.2*. The ARI corresponding to the NMSPE minimum was labelled ARI_{PM}.

3. Experimental protocol and data analysis

3.1 Experimental protocol

Data belong to an historical database built to study cardiovascular and cerebrovascular control responses to orthostatic challenge in individuals prone to develop postural syncope via the analysis of spontaneous fluctuations of physiological variables (Faes et al., 2013; Bari et al., 2016). In this study we considered 13 subjects with previous history of unexplained syncope (SYNC, age: 28 ±9 yrs; 5 males) and 13 healthy control subjects with no previous history of syncope (nonSYNC, age: 27 ± 8 yrs; 5 males). SYNC group had more than 3 events of syncope in the previous 2 years and the event could be reproduced in laboratory via head-up tilt testing. Physical examination, neurological evaluation including magnetic resonance imaging, standard laboratory tests, 12 lead electrocardiogram, 24h Holter assessment, blood pressure monitoring, bilateral carotid artery flow evaluation and standard echocardiography were utilized to exclude obvious causes of syncope in SYNC group. The status of nonSYNC subjects were typified via physical evaluation and full neurological assessment. The two age- and gender-matched groups were enrolled at the Neurology Division of Sacro Cuore Hospital, Negrar, Italy. The study adhered to the principles of the Declaration of Helsinki for medical research involving humans. Local ethical committee approved the study. All subjects gave written informed consent before performing the experimental session. Subjects were instructed to avoid caffeinated and alcoholic beverages for 24h before the study. None of nonSYNC and SYNC individuals were taking any medication affecting cardiovascular control. Experiments took place in the morning in a temperature-controlled room. Subjects were

instrumented to continuously monitor the electrocardiogram (ECG) from lead II and AP via a volume clamp device from the middle finger of the right hand (Finapres Medical Systems, Enschede, The Netherlands). CBF velocity measured from the middle cerebral artery through a transcranial Doppler device (Multi-Dop T, DWL, 2MHz, Compumedics, San Juan Capistrano, CA, USA) was taken as a proxy of CBF. CBF velocity signal were low-pass filtered with a sixth-order Butterworth filter with cut-off frequency of 10 Hz. The signals were acquired synchronously at a sampling rate of 1000 Hz. After having instrumented the subject a period of 5 minutes was left for stabilization of physiological variables. The subjects underwent 10 minutes of recording at rest in supine position (REST) followed by head-up tilt test with tilt table inclination of 60° (TILT). The maximum duration of the TILT session was set to 40 min. Prolonged TILT induced signs of presyncope in all SYNC subjects with a different timing. When these signs were observed the subject was returned to REST and the symptoms disappeared. None of the nonSYNC subjects exhibited presyncope signs.

3.2 Beat-to-beat series extraction

HP was computed from the ECG as the time interval between two consecutive R-wave peaks. The *k*th systolic AP (SAP) was defined as the maximum AP value within the *k*th HP. Diastolic arterial pressure (DAP) was detected as the minimum AP value after the *k*th SAP. The *k*th MAP was computed as the ratio of the definite integral of AP between the (*k*–1)th and *k*th DAP occurrences to the interdiastolic interval. The same procedure was applied to CBF velocity to compute MCBFV and the fiducial points for the computation of the definite integral were exactly the same (Faes et al., 2013; Bari et al., 2016).

In order to study short-term regulatory mechanisms, we selected sequences of 250 consecutive synchronous MAP and MCBFV values (Task Force, 1996) at random positions within the REST and TILT sessions. The first minute of TILT session just after the change of the inclination of the tilt table were excluded to avoid sequences featuring transitory adjustments of the variables (Claassen et al., 2016). The selection of TILT segments occurs within the first 10 minutes from the TILT onset. The period of analysis during TILT of the SYNC and nonSYNC group started 260±180 s after the TILT onset with no significant between-group difference. The syncope occurred after 1047±546 s from the TILT onset in SYNC subjects. Time domain markers such as mean and variance of HP, SAP, MAP and MCBFV were computed and labelled, respectively, μ_{HP}, σ^2_{HP}, μ_{SAP}, σ^2_{SAP}, μ_{MAP}, σ^2_{MAP}, μ_{MCBFV} and σ^2_{MCBFV}. They were expressed in ms, ms^2, mmHg, $mmHg^2$, mmHg, $mmHg^2$, $cm \cdot s^{-1}$, and $cm^2 \cdot s^{-2}$. Missing values owing to overlooked detections of the R-wave peak were manually inserted. Misdetections linked to the occasional spikes of noise on the ECG trace

were deleted. If an HP could be measured, the associated SAP, MAP and MCBFV values were always extracted. The effect of ectopic beats or isolated arrhythmic events were mitigated via linear interpolation between the closest values unaffected by arrhythmic beat. Corrections did not exceed 5% of the total sequence length.

3.3 Frequency domain markers of ANS from HP and SAP variabilities

We performed parametric power spectral analysis based on the best fitting of the series with an autoregressive (AR) model regressing current series value on its own past (Task Force, 1996). The coefficients of the AR model and the variance of the white noise were identified directly from the series by solving the least squares problem via Levinson-Durbin recursion (Kay and Marple, 1981). The number of coefficients was chosen according to the Akaike's figure of merit in the range from 10 to 16 (Akaike, 1974). Power spectral density was computed from the coefficients of the model and from the variance of the prediction error (Kay and Marple, 1991). Power spectral density was factored into spectral components being each of them characterized by a central frequency (Baselli et al., 1997). A spectral component was labeled as low frequency (LF) if its central frequency was between 0.04 and 0.15 Hz, whereas it was classified as high frequency (HF) if its central frequency was between 0.15 and 0.4 Hz (Task Force, 1996). The LF and HF powers were defined as the sum of the powers of all LF and HF spectral components, respectively. The following spectral indexes were computed: 1) HF power of the HP series (HFa_{HP}) expressed in absolute units taken as a marker of vagal modulation directed to the sinus node (Pomeranz et al., 1985); 2) the LFa_{HP}/HFa_{HP} ratio, obtained by dividing the LF by the HF powers computed over HP series, deemed to be an indicator of the sympatho-vagal balance to the heart (Montano et al., 1994); 3) the LF power of SAP (LFa_{SAP}) expressed in absolute units (i.e., $mmHg^2$) considered to be an index of sympathetic modulation directed to the vessels (Pagani et al., 1997).

3.4 Frequency domain markers from MAP and MCBFV variabilities

AR power spectral analysis was applied to MAP and MCBFV series as well. Procedure for the identification of the coefficients of the AR model and optimization of the model order was the same utilized to compute spectral indexes of HP and SAP series. The power was calculated in the traditional bands optimized to describe cerebrovascular regulation, namely very low frequency (VLF) from 0.02 to 0.07 Hz, LF from 0.07 to 0.2 Hz and HF from 0.2 to 0.4 Hz bands (Claassen et al., 2016). The powers of the MAP and MCBFV series were expressed in absolute units, namely $mmHg^2$ and $cm^2 \cdot s^{-2}$ respectively, and labelled $VLFa_{MAP}$, $VLFa_{MCBFV}$, LFa_{MAP}, LFa_{MCBFV}, HFa_{MAP} and HFa_{MCBFV}.

3.5 Identification of the ARX model from MAP and MCBFV variabilities

The coefficients of the ARX model were identified by solving traditional least squares approach via Cholesky decomposition method (Baselli et al., 1997). The model order p was optimized in the range from 4 to 14 according to the extension of the Akaike's figure of merit to bivariate processes (Akaike, 1974). The whiteness of the prediction errors of MCBFV and its mutual uncorrelation, even at zero lag, with the MAP series were checked in correspondence of the optimal model order (Baselli et al., 1997; Porta et al., 2000). The fulfillment of these two requirements was taken as a marker of the suitability of the ARX model in describing the MCBFV-MAP dynamic interactions.

3.6 Surrogate data analysis

For each MAP and MCBFV matched pair a surrogate couple was generated by associating a MCBFV series taken from one subject with a MAP series taken from a different subject drawn at random within the same experimental session (i.e. REST or TILT) and group (i.e. SYNC or nonSYNC). One surrogate pair of MAP and MCBFV series was created for each matched couple. We hypothesize that unmatched pairs destroy the physiological level of coupling present in matched couples and the exploited procedures for ARI estimation could detect this unphysiological condition at least in the experimental condition and group where this situation is unlikely (e.g. in nonSYNC at REST), thus guaranteeing that the estimate of ARI provided by the considered method (i.e. TDM, nonPM and PM) is reliable enough.

3.7 Statistical analysis

Two-way repeated measures analysis of variance (one factor repetition, Holm-Sidak test for multiple comparison) was utilized to assess the significance of the differences between original or surrogate series within the same experimental condition (i.e. REST or TILT) and between experimental condition within the same type of data (i.e. original or surrogate series). The same test was employed to check the significance of the differences between experimental condition within the same group (i.e. nonSYNC or SYNC) and between groups within the same experimental condition (i.e. REST or TILT). χ^2 test was applied to the proportion of subjects with ARI_{TDM} or ARI_{PM} larger than 4 to assess the effect of TILT within an assigned group and the different behavior of nonSYNC and SYNC within the same experimental condition. The level of significance of the test (i.e. 0.05) was lowered according to the number of comparisons (i.e. 4) to account for the multiple comparison issue. The association between ARI_{TDM} and ARI_{PM} was checked via Pearson

correlation analysis over the pooling of data regardless of experimental condition and group. Pearson product moment correlation coefficient *r* and type I error probability *p* were calculated. Paired t test, or Wilcoxon signed rank test if appropriate, was utilized to check the constant bias between ARI_{TDM} and ARI_{PM}. Continuous variables are reported as mean ± standard deviation. Statistical analysis was performed with a commercial statistical software (Sigmaplot v.14.0, Systat Software, San Jose, CA, USA). A value of type I error probability $p<0.05$ was always deemed as significant.

4. Results

Table 1 reports time domain indexes computed over HP, SAP, MAP and MCBFV series at REST and during TILT in both nonSYNC and SYNC groups. The effect of TILT was visible over μ_{HP} and μ_{MCBFV} in both nonSYNC and SYNC groups and over σ^2_{HP} and μ_{MAP} only in SYNC individuals. More specifically, during TILT μ_{HP} and μ_{MCBF} decreased significantly in both groups, σ^2_{HP} diminished significantly only SYNC and μ_{MAP} raised significantly only SYNC. The two groups could not be distinguished within the same experimental session with the notable exception of μ_{MAP} at REST that was lower in SYNC than in nonSYNC subjects.

Table 2 reports frequency domain indexes computed over HP and SAP series, traditionally utilized to typify the ANS state, at REST and during TILT in both nonSYNC and SYNC groups. The effect of TILT was visible over LF_{HP}/HF_{HP} in both nonSYNC and SYNC groups, over HF_{HP} only in SYNC individuals and over LF_{SAP} only in nonSYNC subjects. More specifically, during TILT LF_{HP}/HF_{HP} increased significantly in both groups, HF_{HP} diminished significantly only SYNC and LF_{SAP} raised significantly only nonSYNC. Within the same experimental session, no significant differences were found between groups.

Table 3 reports frequency domain indexes expressed in absolute units computed over MAP and MCBFV at REST and during TILT in both nonSYNC and SYNC groups. TILT induced a significant raise of LF_{MAP} in both groups and a significant increase of LF_{MCBFV} exclusively over nonSYNC individuals. None of the spectral indexes computed over MAP and MCBFV series were able to distinguish nonSYNC from SYNC subjects within the same experimental session.

The vertical grouped error bar graphs of Fig.1 shows $NMSPE_{TDM}$ computed between the best matching between the real MCBFV series and the MCBFV version generated via the Tiecks' model as a function of the experimental condition (i.e. REST and TILT). $NMSPE_{TDM}$ indexes were computed over the original (solid black bars) and over surrogate (solid white bars) pairs in nonSYNC (Fig.1a) and SYNC (Fig.1b) subjects. Regardless of the experimental condition, $NMSPE_{TDM}$ calculated over the original pairs was significantly smaller than that computed over

surrogate couples (Figs.1a,b). Over the original data $NMSPE_{TDM}$ was smaller during TILT than at REST, while no between-session differences were detected over surrogates (Figs.1a,b). These conclusions held in both nonSYNC (Fig.1a) and SYNC (Fig.1b) groups.

The vertical grouped error bar graphs of Fig.2 shows $NMSPE_{nonPM}$ (Figs.2a,b) and $NMSPE_{PM}$ (Figs.2c,d) computed between the best matching between the impulse response derived from nonPM and the one generated via the Tiecks' model. NNSPE markers were calculated over the original (solid black bars) and surrogate (solid white bars) series as a function of the experimental condition (i.e. REST and TILT). Results derived from nonSYNC and SYNC groups are reported in Figs.2a,c and Figs.2b,d respectively. $NMSPE_{nonPM}$ did not vary across either experimental conditions and types of series (Figs.2a,b). This finding held in both nonSYNC (Fig.2a) and SYNC (Fig.2b) individuals. In SYNC group $NMSPE_{PM}$ was significantly smaller when computed over original pairs than surrogate couples regardless of the experimental condition (Fig.2c). In nonSYNC individuals this result was observed exclusively at REST (Fig.2d). Assigned the type of series the effect of TILT over $NMSPE_{PM}$ was not visible in either nonSYNC and SYNC individuals (Figs.2c,d).

Figure 3 shows the ARI_{TDM} (Fig.3a) and the percentage of subjects with $ARI_{TDM}>4$ (Fig.3b) computed as a function of the experimental condition (i.e. REST and TILT) in nonSYNC (solid black bar) and SYNC (solid white bars) groups. Both ARI_{TDM} and the percentage of subjects with $ARI_{TDM}>4$ did not vary with experimental condition and group. Figure 4 has the same structure as Fig.3 but it shows results relevant to the ARI_{PM}. Like in Fig.3 markers did not vary with experimental condition and group.

ARI_{TDM} was significantly and positively associated with ARI_{PM} with r=0.405 and $p=2.88\times10^{-3}$. However, when ARI_{TDM} and ARI_{PM} were directly compared (Fig.5), the lower values of ARI_{TDM} compared to ARI_{PM} suggested that the two ARI estimates were not interchangeable and a constant bias was present.

5. Discussion

The main findings of this study can be summarized as follows: i) TDM and PM exhibited a greater statistical power in differentiating original matched and surrogate unmatched sequences than nonPM; ii) although TDM and PM led to ARI estimates significantly correlated, ARI_{TDM} and ARI_{PM} were not interchangeable; iii) ANS response to postural stressor was different in nonSYNC and SYNC groups; iv) orthostatic challenge did not affect CA of either nonSYNC or SYNC group.

5.1 TDM and PM are more powerful in separating original and surrogate pairs than nonPM

In the present study we exploited three approaches to the assessment of CA based on the evaluation of ARI derived from Tiecks' differential equations (Tiecks et al., 1995) applied to spontaneous MAP and MCBFV variability. The first technique, labelled TDM, is grounded on the comparison between the MCBFV time course predicted from the Tiecks' model fed by the original MAP and the real MCBFV series (Mahdi et al., 2017; Lee et al., 2020). The second approach, categorized nonPM, is based on the comparison between the impulse response of the Tiecks' model and the one estimated in the frequency domain according to nonparametric cross-spectral analysis (Panerai et al., 1998). The third approach, labelled PM, is based on the comparison between the impulse response of the Tiecks' model and the one derived from the identification of a parametric model (Panerai et al., 1999; Simpson et al., 2001; Dineen et al., 2010) belonging to the ARX class (Porta et al., 2000; Porta et al., 2018). In all the methods, i.e. TDM, nonPM and PM, the Tiecks' model was parametrized according to 10 sets of parameters that were ranked according to ARI classes ranging from 0 to 9 representing different CA states. The ARI class leading to the best agreement with data, as measured via NMSPE, was selected. All the approaches were applied to original matched and surrogate unmatched MAP and MCBFV pairs. The methods were graded according to their ability in separating original and surrogate pairs under the hypothesis that unmatched surrogate couples set a degree of coupling between MAP and MCBFV that was too weak to be considered physiologically plausible when CA was working.

Since TDM and PM were capable to separate original matched and surrogate unmatched pairs, solely those methods were adopted for the subsequent estimation of ARI, namely ARI_{TDM} and ARI_{PM} in this study. The nonPM featured a much more limited statistical power, mainly due to the dramatic dispersion of NMSPE values. This finding held over both original matched and surrogate unmatched couples. While the high level of ARI_{nonPM} variability could be expected over unmatched surrogate couples, it is surprising the same dispersion of ARI_{nonPM} was found over the original matched pairs. This enormous dispersion of nonPM might be due to the sensitivity of this method to noise realizations superposed to both MAP and MCBFV series. Indeed, nonparametric transfer function estimation procedure does not feature any dampening ability over noise, thus leaving the corresponding impulse response largely affected by artifacts and favoring the dispersion of NMSPE. Conversely, noise might be limited by TDM as a result of the Tiecks' model high-pass characteristic naturally reducing slow trends of MCBFV and by PM as a result of the small number of coefficients of the ARX model. Therefore, when the target is the computation of ARI from spontaneous MAP and MCBFV variability series, TDM and PM should be preferred with respect to nonPM.

5.2 TDM and PM provide different ARI estimates

Although ARI_{TDM} and ARI_{PM} are significantly correlated, they cannot be considered indistinguishable. Indeed, ARI_{PM} was significantly higher than ARI_{TDM}, thus indicating a constant bias between the two ARI estimates. This finding might be the consequence of the better ability of TDM in accounting the actual degree of coupling between MAP and MCBFV. After estimating the transfer function via the PM, the actual level of association between MAP and MCBFV is completely disregarded by the PM because the estimated transfer function did not account explicitly for the goodness of fit. This attitude of the PM might have favored the description of an intermediate level of correlation between MAP and MCBFV with a limited variability of ARI_{PM}. The most frequently detected values of ARI_{PM} is 7 and it was found 67% of the analyses. Conversely, the actual level of association between MAP and MCBFV was always taken into account by ARI_{TDM} because MCBFV was computed by feeding the model with MAP and by observing the MCBFV responses, thus allowing a more faithful reproduction of the actual magnitude of link between MAP and MCBFV. As a consequence, ARI_{TDM} seems to be more flexible in describing the physiological variability of the CA. The most frequently detected value of ARI_{TDM} is 6 and it was found 38% of the analyses. More importantly the $ARI_{TDM}=0$ was found in 13% of the analyses, while $ARI_{PM}=0$ was found in 2%. Given this greater flexibility we recommend the use of TDM for the ARI estimation derived from Tiecks' differential equations.

5.3 nonSYNC and SYNC subjects exhibit different ANS responses to orthostatic challenge

Both nonSYNC and SYNC individuals responded with a tachycardia to the orthostatic challenge. In spite of this similar changes of μ_{HP} to TILT, ANS markers featured subtle between-group differences. Indeed, the well-known vagal withdrawal associated to the postural challenge (Montano et al., 1994; Cooke et al., 1999; Furlan et al., 2000, Marchi et al., 2016) was more evident in SYNC individuals given that solely on SYNC group the HFa_{HP} decreased significantly during TILT. Moreover, the well-known sympathetic activation associated to the orthostatic stressor (Montano et al., 1994; Cooke et al., 1999; Furlan et al., 2000, Marchi et al., 2016) was more evident in nonSYNC individuals given that solely in nonSYNC group the LFa_{SAP} raised significantly during TILT. These subtle differences of ANS control and the link between ANS and CA (Zhang et al., 2002; Ogoh et al., 2008; Hamner et al., 2010) prompt to check whether CA markers could reflect in some way the different state of ANS in the two groups.

5.4 Orthostatic challenge does not affect the CA of either nonSYNC or SYNC group

It is well-known that orthostatic stressor produces the decrease of μ_{MCBFV} (Grubb et al., 1991; Levine et al., 1994; Zhang et al., 1998; Carey et al., 2001; Castro et al., 2017). This decrease is considered to be the consequence of the modification of the ANS state leading to the increase of cerebrovascular resistances in the presence of an active CA that keeps the CBF steady. Since values of μ_{MCBFV} were modified similarly during TILT in both nonSYNC and SYNC groups in presence of greater changes of μ_{MAP} in SYNC individuals, static component of CA seems to suggest some differences between the two groups. Conversely, the maintenance of σ^2_{MAP} and σ^2_{MCBFV} during TILT points toward a preservation of the dynamic component of CA in both groups. This result suggests similar ability of the two groups in counteracting to MAP changes with suitable variations of cerebrovascular resistances such a way to keep CBF variability to the level observed at REST. The result was confirmed even when spectral indexes of MAP and MCBFV variability were computed in a range of frequencies that might be more under ANS control, namely above 0.05 Hz (Hammer et al., 2010). Indeed, the raise of LF_{MCBFV} power during TILT compared to REST can be explained by the increase of LF_{MAP} index in both groups, thus leaving unmodified the change of MCBFV per unit variation of MAP. Thus, as to the dynamic component of the CA nonSYNC and SYNC individuals can be considered to be indistinguishable. This conclusion was confirmed when both ARI and the percentages of subjects with ARI>4 were considered. Remarkably, this conclusion was particularly robust given that it held for both ARI_{TDM} and ARI_{PM}. This finding indicates that the different ANS states characterizing nonSYNC and SYNC groups did not produce significant influences on dynamic component of CA in the early phase of TILT. When nonSYNC and SYNC group were pooled together the effect of TILT on ARI and percentage of subjects with ARI>4 was undetectable, thus suggesting the dynamic component of CA was preserved during orthostatic challenge in spite of the new state of ANS. We remark that the latter conclusion is in agreement with the one obtained via a PM exploiting different class of models with respect to the ARX one (Castro et al., 2017). This conclusion is in agreement with the one based on estimation of frequency domain markers derived from the MCBFV-MAP transfer function (Schondorf et al., 2001). Given that some differences between the two groups were detected using a model-based technique assessing the strength of directional interactions from MAP to MCBFV (Bari et al., 2017), future works should clarify whether different approaches to the evaluation of the MCBFV-MAP relationship might describe different aspects of CA.

6. Conclusions

The method based on the direct comparison of the recorded MCBFV variability with the version predicted from the Tiecks' model should be preferred to approaches comparing the impulse

response of the Tiecks' model to that derived from either nonparametric or parametric transfer function estimated from the real variability. Indeed, the former technique features a good statistical discriminative power in separating the physiological level of MCBFV-MAP coupling from full uncoupling and appears to preserve a sufficient flexibility in describing the physiological variability of CA states. The application of this procedure suggested that CA is preserved during sympathetic activation and vagal withdrawal imposed by a postural stressor and this preservation held even in subjects prone to developed postural syncope in the early phase of the orthostatic challenge. We conclude that the analysis of MCBFV-MAP dynamic interactions cannot be exploited to predict people at risk to develop postural syncope. Future studies should assess whether the time varying application of the approach could follow the derangement of CA during the postural challenge and could indicate the time of the syncope sufficiently in advance. Moreover, since postural challenge induces a sizable ANS response and this response is different in nonSYNC and SYNC groups, the lack of changes of CA markers suggests that ANS changes might not directly imply CA modifications.

References

Aaslid, R., Lindegaard, K.F., Sorteberg, W., et al., 1989. Cerebral autoregulation dynamics in humans. Stroke. 20, 45–52.

Akaike, H., 1974. A new look at the statistical novel identification. IEEE Trans. Automat. Contr. 19, 716–723.

Angarita-Jaimes, N., Kouchakpour, H., Liu, J., et al., 2010. Optimising the assessment of cerebral autoregulation from black box models. Med. Eng. Phys. 36, 607–612.

Bari, V., Marchi, A., De Maria, B., et al., 2016. Nonlinear effects of respiration on the crosstalk between cardiovascular and cerebrovascular control systems. Phil. Trans. R. Soc. A 374, 20150179.

Bari, V., De Maria, B., Mazzucco, C.E., et al., 2017. Cerebrovascular and cardiovascular variability interactions investigated through conditional joint transfer entropy in subjects prone to postural syncope. Physiol. Meas. 38, 976–991.

Baselli, G., Porta, A., Rimoldi, O., et al., 1997. Spectral decomposition in multichannel recordings based on multivariate parametric identification. IEEE Trans. Biomed. Eng. 44, 1092–1101.

Bondar, R.L., Kassam, M.S., Stein, F., et al., 1995. Simultaneous cerebrovascular and cardiovascular responses during presyncope. Stroke. 26, 1794–1800.

Carey, B.J., Manktelow, B.N., Panerai, R.B., et al., 2001. Cerebral autoregulatory responses to head-up tilt in normal subjects and patients with recurrent vasovagal syncope. Circulation. 104, 898-902.

Carey, B.J., Panerai, R.B., Potter, J.F., 2003. Effect of aging on dynamic cerebral autoregulation during head-up tilt. Stroke. 34, 1871–1875.

Castro, P.M., Santos, R., Freitas, J., et al., 2014. Autonomic dysfunction affects dynamic cerebral autoregulation during Valsalva maneuver: comparison between healthy and autonomic dysfunction subjects. J. Appl. Physiol. 117, 205-213.

Castro, P., Freitas, J., Santos, R., et al., 2017. Indexes of cerebral autoregulation do not reflect impairment in syncope: insights from head-up tilt test of vasovagal and autonomic failure subjects. Eur. J Appl. Physiol. 117, 1817–1831.

Cassaglia, P.A., Griffiths, R.I., Walker, A.M., 2008. Sympathetic nerve activity in the superior cervical ganglia increases in response to imposed increases in arterial pressure. Am. J. Physiol. 294, R1255–R1261.

Claassen, J.A., Meel-van den Abeelen, A.S., Simpson, D.M., et al., on behalf of the International Cerebral Autoregulation Research Network (CARNet). 2016. Transfer function analysis of dynamic cerebral autoregulation: A white paper from the International Cerebral Autoregulation Research Network. J. Cereb. Blood Flow Metab. 36, 665–680.

Cooke, W.H., Hoag, J.B., Crossman, A.A., et al., 1999. Human responses to upright tilt: a window on central autonomic integration. J. Physiol. 517, 617–628.

Dineen, N.E., Brodie, F.G., Robinson, T.G., et al., 2010. Continuous estimates of dynamic cerebral autoregulation during transient hypocapnia and hypercapnia. J. Appl. Physiol. 108, 604–613.

Faes, L., Porta, A., Rossato, G., et al., 2013. Investigating the mechanisms of cardiovascular and cerebrovascular regulation in orthostatic syncope through an information decomposition strategy. Auton Neurosci: Basic Clin. 178, 76–82.

Folino, A.F., Russo, G., Porta, A., et al., 2007. Modulations of autonomic activity leading to tilt-mediated syncope. Int. J. Cardiol. 120, 102–107.

Furlan, R., Porta, A., Costa, F., et al., 2000. Oscillatory patterns in sympathetic neural discharge and cardiovascular variables during orthostatic stimulus. Circulation. 101, 886–892.

Furlan, R., Heusser, K., Minonzio, M., et al., 2019. Cardiac and vascular sympathetic baroreflex control during orthostatic pre-syncope. J. Clin. Med. 8, 1434.

Grubb, B.P., Gerard, G., Roush, K., et al., 1991. Cerebral vasoconstriction during head-upright tilt-induced vasovagal syncope: a paradoxic and unexpected response. Circulation. 84, 1157–1164.

Hamner, J.W., Tan, C.O., Lee, K., et al., 2010. Sympathetic control of the cerebral vasculature in humans. Stroke 41, 102–109.

Kay, S.M., Marple, S.L., 1981. Spectrum analysis: a modern perspective. Proc. IEEE. 69, 1380–1418.

Kety, S.S., Schmidt, C.F., 1948. The nitrous oxide method for the quantitative determination of cerebral blood flow in man: theory, procedure and normal values. J. Clin. Invest. 29, 476–483.

Kontos, H.A., 1989. Validity of cerebral arterial blood flow calculations from velocity measurements. Stroke. 20, 1–3.

Lassen, N.A., 1959. Cerebral blood flow and oxygen consumption in man. Physiol. Rev. 39, 183–238.

Lee, Y.-K., Rothwell, P.M., Payne, S.J., et al., 2020. Reliability, reproducibility and validity of dynamic cerebral autoregulation in a large cohort with transient ischaemic attack or minor stroke. Physiol. Meas. 41, 095002.

Lefthériotis, G., Preckel, M.P., Fizanne, L., et al., 1998. Effect of head-upright tilt on the dynamic of cerebral autoregulation. Clin Physiol. 18, 41–47.

Levine, B.D., Giller, C.A., Lane, L.D., et al. 1994. Cerebral versus systemic hemodynamics during graded orthostatic stress in humans. Circulation. 90, 298–306.

Liu, X., Czosnyka, M., Donnelly, J., et al., 2020. Assessment of cerebral autoregulation indexes - a modelling perspective. Sci. Rep. 10, 9600.

Mahdi, A., Nikolic, D., Birch, A.A., et al., 2017. Increased blood pressure variability upon standing up improves reproducibility of cerebral autoregulation indexes. Med. Eng. Phys. 47, 151–158.

Marchi, A., Bari, V., De Maria, B., et al., 2016. Calibrated variability of muscle sympathetic nerve activity during graded head-up tilt in humans and its link with noradrenaline data and cardiovascular rhythms. Am. J. Physiol. 310, R1134–R1143.

Montano, N., Gnecchi-Ruscone, T., Porta, A., et al., 1994. Power spectrum analysis of heart rate variability to assess changes in sympatho-vagal balance during graded orthostatic tilt. Circulation. 1994; 90, 1826–1831.

Obrist, W.D., Thompson, H.K., Wang, H.S., et al., 1975. Regional cerebral blood flow estimated by ^{133}Xenon inhalation. Stroke. 6, 245–256.

Ogoh, S., Brothers, R.M., Eubank, W.L., et al., 2008. Autonomic neural control of the cerebral vasculature: acute hypotension. Stroke. 39, 1979–1987.

Pagani, M., Montano, N., Porta, A., et al., 1997. Relationship between spectral components of cardiovascular variabilities and direct measures of muscle sympathetic nerve activity in humans. Circulation. 95, 1441–1448.

Panerai, R.B., White, R.P., Markus, H.S., et al., 1998. Grading of cerebral dynamic autoregulation from spontaneous fluctuations in arterial blood pressure. Stroke. 29, 2341–2346.

Panerai, R.B., Dawson, S.L. Potter, J.F., 1999. Linear and nonlinear analysis of human dynamic cerebral autoregulation. Am. J. Physiol. 277, H1089–H1099.

Panerai, R.B., Dawson, S.L., Eames, P.J., et al., 2001. Cerebral blood flow velocity response to induced and spontaneous sudden changes in arterial blood pressure. Am. J. Physiol. 280, H2162–H174.

Piccirillo, G., Naso, C., Moisè, A., et al., 2004. Heart rate and blood pressure variability in subjects with vasovagal syncope. Clin. Sci. 107, 55–61.

Pomeranz, B., Macaulay, R.J., Caudill, M.A., et al., 1985. Assessment of autonomic function in humans by heart rate spectral analysis. Am. J. Physiol. 248: H151–H153.

Porta, A., Baselli, G., Rimoldi, O., et al., 2000. Assessing baroreflex gain from spontaneous variability in conscious dogs: role of causality and respiration. Am. J. Physiol. 279, H2558–H2567.

Porta, A., Maestri, R., Bari, V., et al., 2018. Paced breathing increases the redundancy of cardiorespiratory control in healthy individuals and chronic heart failure patients. Entropy, 20, 949.

Schondorf, R., Stein, R., Roberts, R., et al., 2001. Dynamic cerebral autoregulation is preserved in neurally mediated syncope. J. Appl. Physiol. 91, 2493–2502.

Simpson, D.M., Panerai, R.B., Evans, D.H., et al., 2001. A parametric approach to measuring cerebral blood flow autoregulation from spontaneous variations in blood pressure. Ann. Biomed. Eng. 29, 18–25.

Task Force of the European Society of Cardiology and the North American Society of Pacing and Electrophysiology, 1996. Heart rate variability: standards of measurement, physiological interpretation and clinical use. Circulation. 93, 1043–1065.

Tiecks, F.P., Lam, A.M., Aaslid, R., et al., 1995. Comparison of static and dynamic cerebral autoregulation measurements. Stroke. 26, 1014–1019.

Tzeng, Y.C., MacRae, B.A., Ainslie, P.N., et al., 2014. Fundamental relationships between blood pressure and cerebral blood flow in humans. J. Appl. Physiol. 117, 1037–1048

Zhang, R., Zuckerman, J.H., Levine, B.D., 1998. Deterioration of cerebral autoregulation during orthostatic stress: insights from the frequency domain. J. Appl. Physiol. 85, 1113–1122.

Zhang, R. Zuckerman, J.H. Iwasaki, K. et al., 2002. Autonomic neural control of dynamic cerebral autoregulation in humans. Circulation. 106, 1814–1820.

Figure captions

Fig.1. The grouped error bar graphs show $NMSPE_{TDM}$ as a function of the experimental condition (i.e. REST and TILT) in nonSYNC (a) and SYNC (b) subjects. $NMSPE_{TDM}$ markers are computed over the original (solid black bars) and surrogate (solid white bars) series. The symbol * indicates significant variations compared to surrogates within the same experimental condition (i.e. REST or TILT) with $p<0.05$. The symbol § indicates significant variations compared to TILT within the same type of series (i.e. original or surrogate sequences) with $p<0.05$.

Fig.2. The grouped error bar graphs show $NMSPE_{nonPM}$ (a,b) and $NMSPE_{PM}$ (c,d) as a function of the experimental condition (i.e. REST and TILT) in nonSYNC (a,c) and SYNC (b,d) subjects. $NMSPE_{nonPM}$ and $NMSPE_{PM}$ markers are computed over the original (solid black bars) and surrogate (solid white bars) series. The symbol * indicates significant variations compared to surrogate within the same experimental condition (i.e. REST or TILT) with $p<0.05$.

Fig.3. The grouped error bar graph (a) shows ARI_{TDM} in nonSYNC (solid black bars) and SYNC (solid white bars) subjects as a function of the experimental condition (i.e. REST and TILT). The grouped bar graph (b) shows the percentage of subjects with $ARI_{TDM}>4$ (i.e. with working CA) in nonSYNC (solid black bars) and SYNC (solid white bars) groups as a function of the experimental condition (i.e. REST and TILT).

Fig.4. The grouped error bar graph (a) shows ARI_{PM} in nonSYNC (solid black bars) and SYNC (solid white bars) subjects as a function of the experimental condition (i.e. REST and TILT). The grouped bar graph (b) shows the percentage of subjects with $ARI_{PM}>4$ (i.e. with working CA) in nonSYNC (solid black bars) and SYNC (solid white bars) groups as a function of the experimental condition (i.e. REST and TILT).

Fig.5. The simple error bar graph shows ARI as a function of the method (i.e. TDM and PM). Data were pooled together regardless of the group (i.e. nonSYNC or SYNC) and experimental condition (i.e. REST or TILT). The symbol § indicates significant variations between ARI_{TDM} and ARI_{PM} with $p<0.05$.

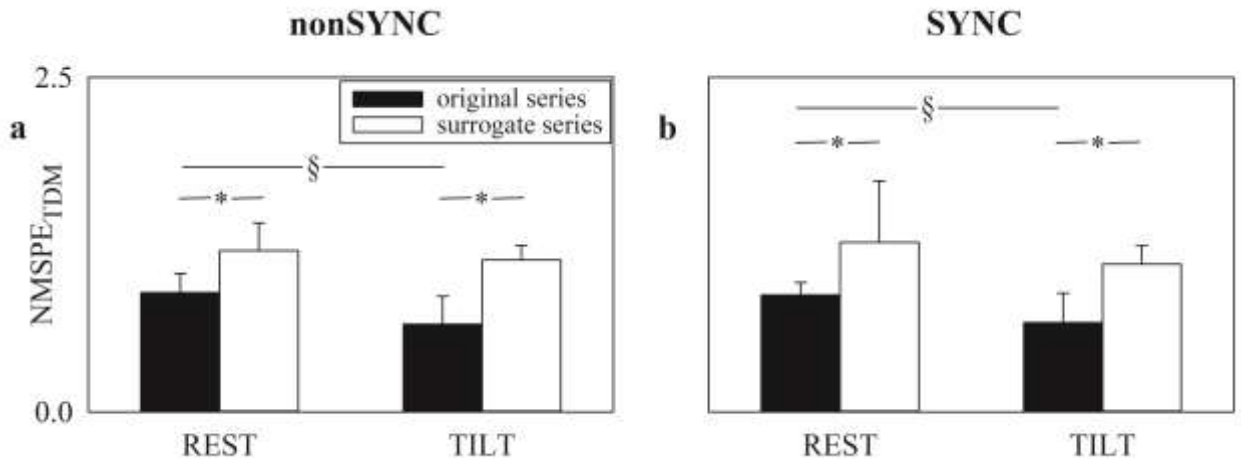
nonSYNC
SYNC
a
b
2.5
0.0
NMSPE$_{TDM}$
original series
surrogate series
§
*
REST
TILT

Fig.1

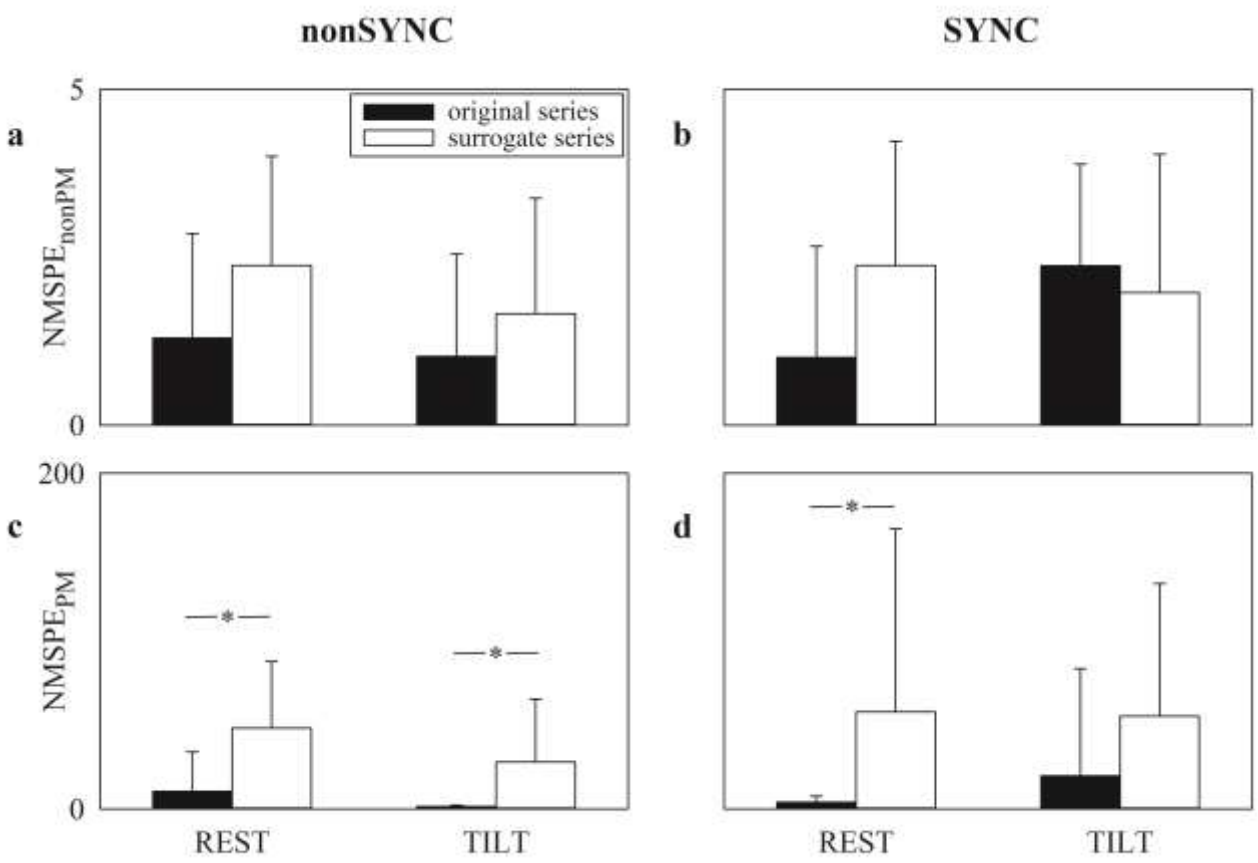
nonSYNC
SYNC
a
b
c
d
5
0
200
0
original series
surrogate series
NMSPE$_{nonPM}$
NMSPE$_{PM}$
*
*
*
REST
TILT
REST
TILT

Fig.2

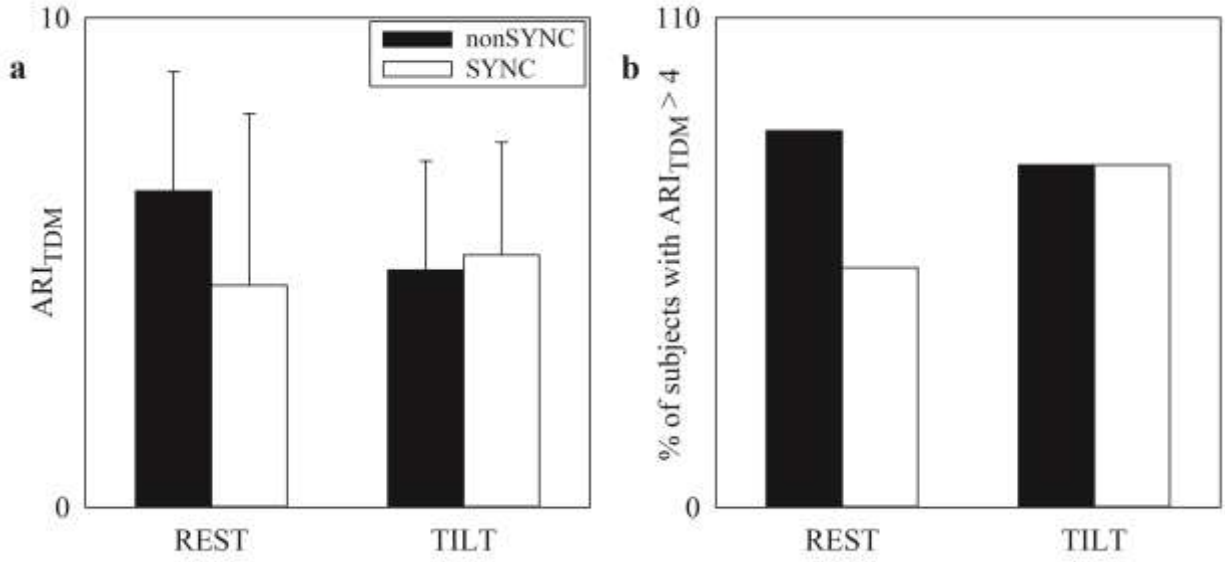
a
10
0
nonSYNC
SYNC
ARI_TDM
REST
TILT
b
110
0
% of subjects with ARI_TDM > 4
REST
TILT

Fig.3

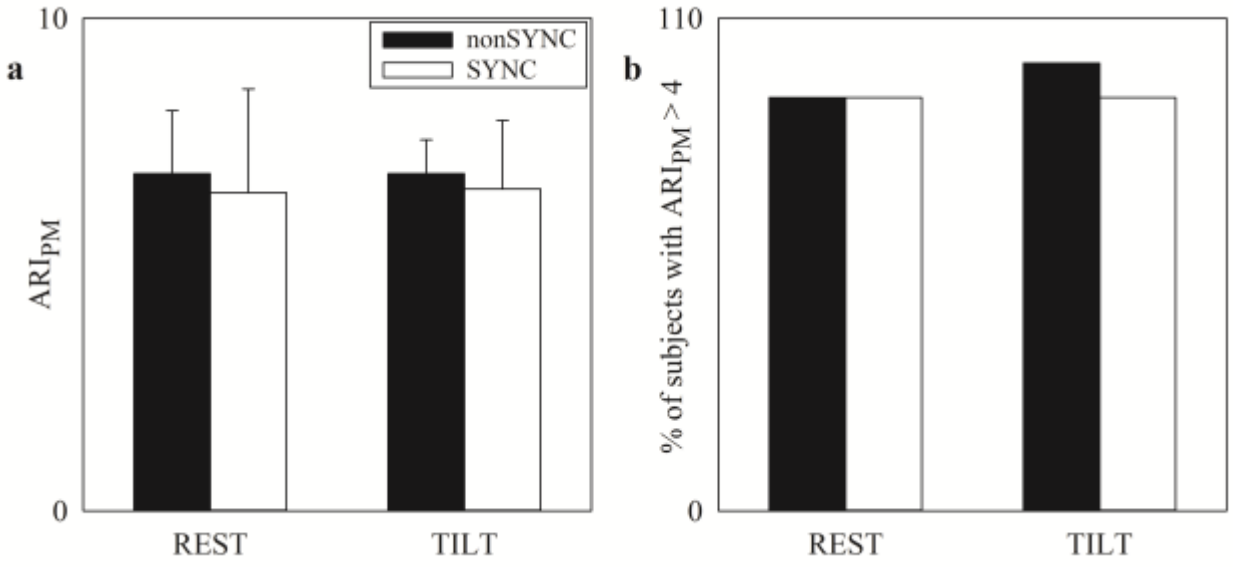
a
10
0
ARI$_{PM}$
nonSYNC
SYNC
REST
TILT
b
110
0
% of subjects with ARI$_{PM}$ > 4
REST
TILT

Fig.4

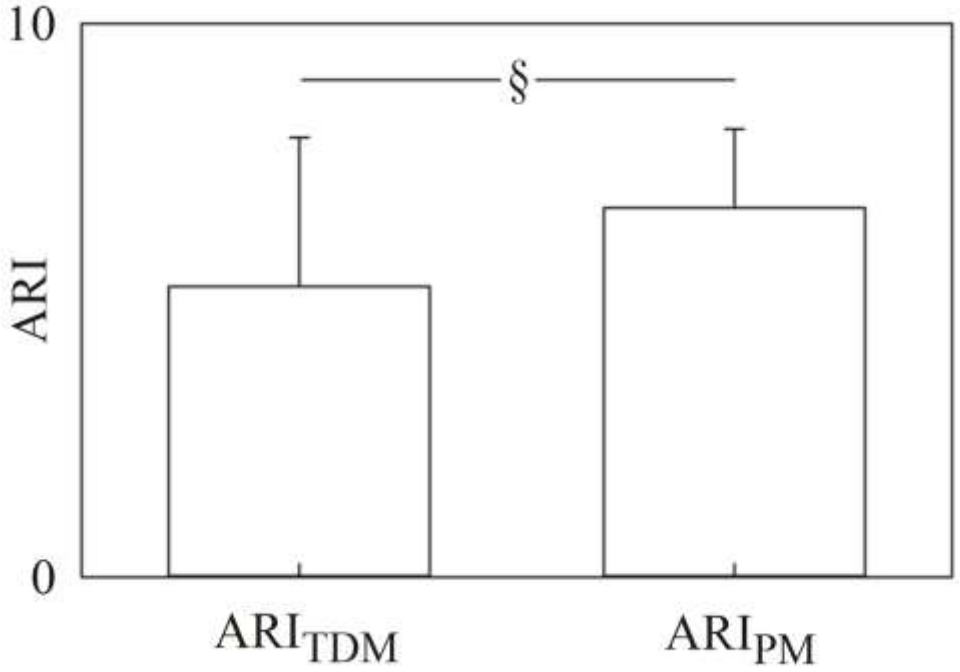

Fig.5

Table 1. Time domain parameters in nonSYNC and SYNC groups at REST and during TILT.

	nonSYNC		SYNC	
	REST	TILT	REST	TILT
μ_{HP} [ms]	848 ± 189	673 ± 108 *	912 ± 143	738 ± 108 *
σ^2_{HP} [ms^2]	2493 ± 2495	1727 ± 1179	4175 ± 3801	2263 ± 1941 *
μ_{SAP} [mmHg]	140 ± 28	135 ± 17	125 ± 21	138 ± 23
σ^2_{SAP} [mmHg^2]	34.59 ± 24.03	43.97 ± 28.80	29.34 ± 20.35	35.75 ± 16.97
μ_{MAP} [mmHg]	99 ± 17	95 ± 12	84 ± 14 §	97 ± 18 *
σ^2_{MAP} [mmHg^2]	20.19 ± 21.59	19.99 ± 11.32	12.30 ± 9.05	16.56 ± 8.10
μ_{MCBFV} [cm·s^{-1}]	72.11 ± 23.14	61.68 ± 21.39 *	52.27 ± 27.96	44.02 ± 28.84 *
σ^2_{MCBFV} [cm^2·s^{-2}]	19.20 ± 12.48	30.73 ± 25.39	30.30 ± 35.79	23.52 ± 27.08

nonSYNC = subjects without a history of recurrent postural syncope; SYNC = subjects with a history of recurrent postural syncope; REST = at rest in supine position; TILT = head-up tilt at 60°; HP = heart period; AP = arterial pressure; SAP = systolic AP; MAP = mean AP; CBF = cerebral blood flow; MCBFV = mean CBF velocity; μ_{HP} = HP mean; σ^2_{HP} = HP variance; μ_{SAP} = SAP mean; σ^2_{SAP} = SAP variance; μ_{MAP} = MAP mean; σ^2_{MAP} = MAP variance; μ_{MCBFV} = MCBFV mean; σ^2_{MCBFV} = MCBFV variance. Data are reported as mean ± standard deviation. The symbol * indicates $p<0.05$ versus REST within the same group. The symbol § indicates $p<0.05$ versus nonSYNC within the same experimental condition.

Table 2. Frequency domain ANS markers from HP and SAP series in nonSYNC and SYNC groups at REST and during TILT.

	nonSYNC		SYNC	
	REST	TILT	REST	TILT
HFa_{HP} [ms^2]	710 ± 1020	208 ± 252	1329 ± 1501	280 ± 534 *
LFa_{HP}/HFa_{HP}	1.97 ± 1.48	5.21 ± 3.68 *	1.53 ± 1.47	6.81 ± 5.75 *
LFa_{SAP} [$mmHg^2$]	4.27 ± 4.81	25.11 ± 31.15 *	5.53 ± 3.89	18.74 ± 12.76

nonSYNC = subjects without a history of recurrent postural syncope; SYNC = subjects with a history of recurrent postural syncope; REST = at rest in supine position; TILT = head-up tilt at 60°; HP = heart period; AP = arterial pressure; SAP = systolic AP; MAP = mean AP; LF = low frequency; HF = high frequency; LFa_{HP} = LF power of the HP series expressed in absolute units; HFa_{HP} = HF power of the HP series expressed in absolute units; LFa_{HP}/HFa_{HF} = the ratio of the LFa_{HP} to HFa_{HP} powers; LFa_{SAP} = LF power of the SAP series expressed in absolute units. Data are reported as mean ± standard deviation. The symbol * indicates $p<0.05$ versus REST within the same group.

Table 3. Frequency domain markers of MAP and MCBFV series in nonSYNC and SYNC groups at REST and during TILT.

	nonSYNC		SYNC	
	REST	TILT	REST	TILT
$VLFa_{MAP}$ [$mmHg^2$]	5.06 ± 8.04	2.53 ± 7.91	2.67 ± 4.83	0.58 ± 2.10
LFa_{MAP} [$mmHg^2$]	6.15 ± 10.56	11.02 ± 10.20 *	4.19 ± 4.18	10.26 ± 7.38 *
HFa_{MAP} [$mmHg^2$]	1.94 ± 1.94	1.70 ± 0.73	1.29 ± 0.79	1.91 ± 1.44
$VLFa_{MCBFV}$ [$cm^2 \cdot s^{-2}$]	9.99 ± 14.92	12.08 ± 24.04	2.79 ± 6.54	0.79 ± 2.06
LFa_{MCBFV} [$cm^2 \cdot s^{-2}$]	3.03 ± 3.37	9.04 ± 8.39 *	6.60 ± 6.81	8.31 ± 6.44
HFa_{MCBFV} [$cm^2 \cdot s^{-2}$]	0.91 ± 0.66	1.82 ± 1.16	1.78 ± 2.03	1.43 ± 1.28

nonSYNC = subjects without a history of recurrent postural syncope; SYNC = subjects with a history of recurrent postural syncope; REST = at rest in supine position; TILT = head-up tilt at 60°; AP = arterial pressure; MAP = mean AP; CBF = cerebral blood flow; MCBFV = mean CBF velocity; LF = low frequency; VLF = very LF; HF = high frequency; $VLFa_{MAP}$ = VLF power of the MAP series expressed in absolute units; LFa_{MAP} = LF power of the MAP series expressed in absolute units; HFa_{MAP} = HF power of the MAP series expressed in absolute units; $VLFa_{MCBFV}$ = VLF power of the MCBFV series expressed in absolute units; LFa_{MCBFV} = LF power of the MCBFV series expressed in absolute units; HFa_{MCBFV} = HF power of the MCBFV series expressed in absolute units; Data are reported as mean ± standard deviation. The symbol * indicates $p<0.05$ versus REST within the same group.